Thermal performance of High-Efficiency Vortex (HEV) variants: reversed arrays configuration

Akram Ghanem, Thierry Lemenand, Dominique Della Valle, Hassan Peerhossaini

Proceedings of the 11th International ISHMT-ASME Heat and Mass Transfer Conference
December 28-31, 2013, IIT Kharagpur, India

Thermal Performance of High-Efficiency Vortex (HEV) Variants: Reversed Arrays Configuration

A. Ghanem[1]*, T. Lemenand[1], D. Della Valle[2], H. Peerhossaini[3]

[1] *LUNAM Université, Laboratoire de Thermocinétique de Nantes, CNRS UMR 6607, 44306 Nantes, France*
[2] *ONIRIS – Nantes, 44322 Nantes, France*
[3] *Université Paris Diderot, Sorbonne Paris Cité, Institut des Energies de Demain (IED), 75013 Paris, France*

Abstract

Convective heat transfer in the Reversed Arrays configuration of the High-Efficiency Vortex (HEV) multifunctional heat exchanger is investigated. An experimental test section constituted of a tube equipped with inclined trapezoidal vortex generators with a constant-flux heating system is designed and constructed. In this configuration, the tab inclination is opposite to the flow direction. Interactions between the tabs and the flow generate coherent structures in the form of longitudinal counter-rotating streamwise vortices enhancing radial particle dispersion, mixing, and ultimately heat transport. The original configuration in which the tabs are inclined in the flow direction is also examined. Recent in-house hydrodynamic and thermal studies have been conducted showing the interest of these configurations in mixing and heat transfer applications. The experimental data are in good agreement with the numerical results. Local Nusselt numbers show an increasing tendency in the longitudinal direction with remarkable cross-sectional variations. Global analysis of convective heat transfer reveals the superiority of the Reversed Arrays. Energy expenditures are assessed through total pressure drop measurements. A comparative analysis based on the thermal enhancement factor and Colburn factor shows that the HEV is energetically less costly than other heat exchangers with similar heat transfer capacity.

Keywords: Heat transfer enhancement, Multifunctional heat exchanger, Vortex generator, Streamwise vorticity

1. Introduction

Streamwise and transverse vortical structures can be artificially generated in turbulent flows by inserting sharp-edged flow perturbators that generate local pressure gradients and shear instabilities [1-4]. These vortices efficiently enhance radial heat and mass transfer and can be used in industrial processes by mounting inclined tabs on the channel wall [5-10]. The main applications are in heat and mass transfer intensification, drag reduction, and control of flow separation in automotive or aeronautic aerodynamics [2,4-6]. Vortex generators can have various geometries and are designed to respond to the specific needs of the desired applications. Their efficiency allows the integration of several operations such as mixing, chemical reaction, and heat transfer into a single system. This implies the definition of multifunctional heat exchangers-reactors: perform the mixing process and chemical reactions simultaneously with the heat exchange [11].

The present experimental study investigates the influence of the trapezoidal tabs used in the classical 'Aligned Arrays' HEV heat exchanger configuration [12] on heat transfer capacity of the device, as well as the effect of their inclination with respect to the flow by examining the 'Reversed Arrays' configuration. Gretta and Smith [1] studied the flow pattern in the Aligned Arrays geometry and identified several types of flow structures induced by the tabs. The main vortical structure created is the counter-rotating vortex pair (CVP) formed in the wake of the tab due to the pressure difference between the low-momentum region under the tab and the high-momentum region above. While propagating downstream, the CVP distorts and splits into hairpin vortex legs because of the instability caused by the difference of vorticity in the vortex core and surrounding fluid. Moreover, when the flow encounters the mixing tab, a three-dimensional shear layer is formed around the tab that becomes more unstable and generates hairpin-like structures, also called horseshoe vortices, riding on top of the CVP and being convected downstream. This phenomenon is caused by the Kelvin–Helmholtz instability in free shear flow [3]. Primary hairpins can further generate secondary vortices in the tab wake [4]. Other secondary instabilities can also occur generating reverse vortices in the tab wake [3,4]. The growth of the hairpin strength is attributed to ejection and entrainment of new vorticity from the near-wall local boundary layer toward the hairpin head [3,4]. Figure 1(a) shows the main generated vortices and flow structures produced in the Aligned Arrays HEV vortical flow.

In a recent numerical study, Habchi *et al.* [13] reported that in the Reversed Arrays, the CVP occupies a larger area of the cross section and extends further into the core flow on both sides of the tab as shown by the streamlines in Fig. 1(c). These three-dimensional streamlines also show the role of the CVP in convecting fluid particles in both radial and streamwise directions and reveal the presence of new vortices. A small necklace vortex forms upstream of a tab inclined in the flow direction. For the reversed tabs, a large necklace vortex emerges at the upper tab edge due to pressure gradients in the direct vicinity of the tab and further enhances mass exchange between the tab wake region

* Corresponding author. Tel.: +33.2.40.68.31.57
E-mail: akram.ghanem@univ-nantes.fr

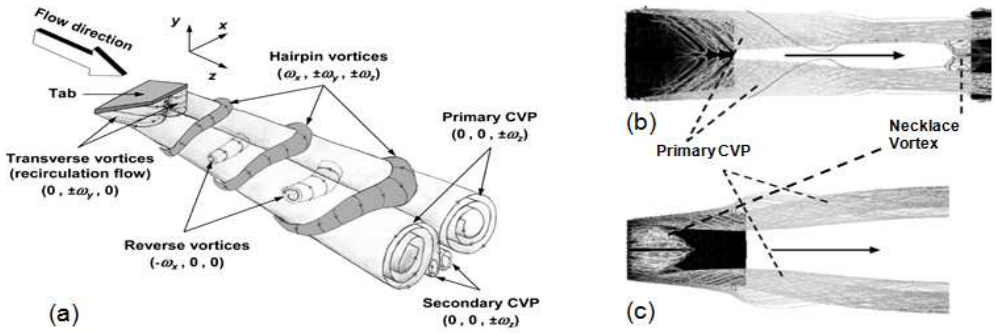

Fig. 1. (a) Flow structure produced downstream of a trapezoidal vortex generator, (b) Streamlines - aligned tab, and (c) Streamlines - reversed tab

and the core flow. In fact, the flow structure changes substantially when the tab inclination is reversed. The CVP vanishes after a certain distance downstream of the tabs because its momentum is damped as it migrates downstream. Examining the magnitude of the velocity vectors, Habchi *et al.* [13] concluded that these vortices are more energetic than those encountered in the Aligned Arrays. The Reversed Arrays configuration significantly enhances micro-mixing and droplet breakup since it presents high local energy dissipation rates, 50% higher than the Aligned Arrays. It also seems to exhibit better meso-mixing performance presenting higher values of turbulent kinetic energy TKE exceeding those of the classical configuration by 25% [13].

In both configurations, interactions between these structures and the main flow significantly enhance mixing by mass exchange between the near-wall region and the core flow [1,3,4]. This mechanism is employed in the HEV heat exchanger, where arrays of trapezoidal tabs produce a complex vortex system [5,6,9,10,14]. These embedded structures contribute to the transfer of momentum, heat and mass that can be analyzed in terms of mixing. More precisely, they specifically contribute to the different scales of mixing in the turbulent flow.

A common application of the multifunctional heat exchanger-reactors studied here is for liquid-liquid dispersion and thermal homogenization in moderate turbulent flows which include exothermal reactions, such as acid catalyzed hydrolysis reactions [11]. These geometries enhance near-wall turbulence preventing fouling, impurity, and local over-heated zones [11].

The aim of this experimental study is to quantify the effect of the hydrodynamic structures on the overall heat transfer performance of both configurations in an attempt to assess the feasibility of the Reversed Arrays HEV as a multifunctional heat exchanger-reactor compared to the classical geometry. The following section describes the experimental rig and the measurement techniques. The results and discussion are presented afterwards, and finally some conclusions are drawn.

2. Experimental apparatus and methods

2.1. Hydraulic Loop and Test Section

The open flow loop in which the experiments are carried out consists of a reservoir from which the working fluid (water at room temperature) is circulated by means of a variable-speed gear pump. The volume flow rate is measured by an electromagnetic flowmeter with an accuracy of 0.25% over the measured range. Upstream of the flowmeter, a high-resolution ball valve is used further to adjust the flow rate after setting the required pump speed to cover the Reynolds numbers, which ranged between 1000 and 50000 corresponding to flow rates between 64 L/h and 3209 L/h. Before entering the test section, the fluid passes through a 2-meter-long straight tube whose length is 100 times its inner diameter, sufficient to ensure a fully developed velocity profile at the inlet of the test section and thus eliminate entrance effects. The circuit is equipped with a safety valve and a pulsation damper to limit any eventual pressure fluctuations produced by the pump and to ensure continuity and stability of flow in the test section.

Figure 2 shows the HEV test section geometry composed of a straight stainless steel tube in the walls of which seven arrays of trapezoidal vortex generators are inserted. Each array is constituted of four tabs inclined at 30° relative to the tube wall. In the Aligned Arrays configuration, the tabs are fixed in the flow direction, while in the Reversed Arrays, they counter the flow, their tips being upstream and their roots downstream. The tube has a length *L* of 168 mm, and a diameter *D* of 22.7 mm and has wall thickness 1.15 mm. The distance between two successive rows of vortex generators is 22 mm, measured at the tab roots. The flow Reynolds number *Re* is defined by:

$$Re = \frac{U_m D}{\nu} \qquad (1)$$

where U_m is the mean axial velocity (ms^{-1}) and ν is the fluid kinematic viscosity ($m^2\ s^{-1}$). Thermophysical properties of water used in the calculation of different quantities are determined at the inlet-outlet average fluid

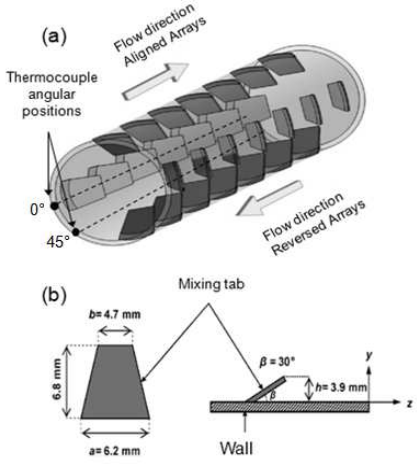

Fig. 2 HEV heat exchanger geometry: (a) global view and (b) tab dimensions

temperature which varies with the flow rate.

2.2. Wall Heating and Temperature Measurement

The HEV heat exchanger is housed inside a stainless steel heating cylinder of 55 mm inner diameter. Figure 3 illustrates the experimental rig with the different components. The outer cylinder is heated by the Joule effect by a continuous heating wire wound around it. Molten tin, with a thermal conductivity λ of 67 $Wm^{-1}K^{-1}$, is cast into the annular gap between the heat exchanger and the heating cylinder with a thickness *e* of 10 mm. After the casting process, the solidified tin ensures perfect contact between the heating surface and the exchanger wall eliminating any thermal contact resistance effects. This indirect heating technique is used to provide a uniform wall heat flux to the heat exchanger. The two ends of the heating wire are connected to a transformer. The electrical output needed to generate a 1100 Watt uniform heat flux in the wire is controlled by adjusting the voltage and the current with a precision of 1%. The constant heat flux provided on the HEV outer wall is calculated from the temperature gradient across the annular gap. For this purpose, temperature is measured at different longitudinal positions by sets of type-K thermocouple beads with an accuracy of ± 0.5 °C, one set welded on the HEV heat exchanger outer wall and the other on the inner wall of the heating tube. There is a total of 4 sets of thermocouples, two are aligned with the tab positions, and two are shifted by 45° and welded at an angular position where there are no tabs fixed to the wall (Fig. 2(a)). This shifted set of thermocouples is necessary to capture the influence of the reversed arrays whose produced vortex pairs are found to spread further into the core flow as discussed above. Thus, there is a total of 46 thermocouples, each pair of which serves as a steady local heat fluxmeter. Calibrated temperature sensors are used to measure the inlet and outlet water temperatures. In a previous study [7], local and global Nusselt numbers in the Aligned Arrays configuration were calculated based on temperature measurements by thermocouples aligned with the tab positions (0°), measuring a constant heat flux traversing thermal grease with a thermal conductivity of 0.7 $Wm^{-1}K^{-1}$. In the present work, the grease is replaced with cast tin with higher conductivity to ensure better heating of the working fluid and reduce relative measurement uncertainties. In addition, the shifted thermocouples give access to a wider zone of the cross-section and provide better estimation of the calculated quantities.

The whole test section is insulated with an Isofrax® thermal insulation blanket fitted with a sensitive heat fluxmeter to measure convective losses. In the experiments, the heat flux at the test section outer wall is set by the transformer and the system is then allowed to reach thermal steady state for each value of flow Reynolds number. Inlet, outlet and longitudinal temperatures are measured continuously *via* an 'Agilent' data acquisition chain and numerically handled using 'BenchLink Data Logger' software. The Fanning friction factor *f* is calculated in terms of pressure drop ΔP (Pa) as measured by three differential manometers covering all head losses with a precision depending on the measured value and varying between 0.1 and 0.25%.

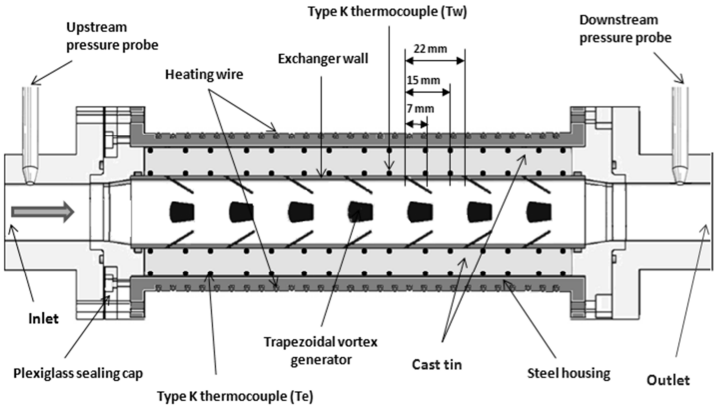

Fig. 3. Test section and aligned thermocouple positions

Experimental uncertainties are evaluated for the derived quantities using the relative errors of measurement of their elementary terms. Repeatability and reproducibility tests are carried out on the experimental results. Standard deviations of the corresponding measurements were calculated to ensure that they are commensurate and abide by research standards.

3. Results and discussion

In this section, the thermal performance in the two HEV configurations is reported for different Reynolds numbers in terms of local Nusselt numbers *Nu*, global Nusselt numbers Nu_g, thermal enhancement factor η, and Colburn factor *j*. The results are compared with those in the literature for turbulent tube flow and other heat exchangers.

3.1. Local Nusselt number

Experiments are run at a constant wall heat flux condition. The heating tube inner wall temperature T_e and the HEV wall temperature T_w, measured in Kelvin (K) at the different longitudinal positions, are used to calculate the local heat flux densities φ (Wm^{-2}) using Eq. (2). The values are found to be scattered around a mean value with 3% maximum deviation.

$$\varphi = \frac{\lambda}{e}(T_e - T_w) \quad (2)$$

From knowledge of the inlet fluid temperature to the heat exchanger, the average fluid temperatures at the entry and exit of each segment are consecutively calculated using a simple energy balance between the heat transferred through the incremental wall surfaces and that transferred to the working fluid. Then these (inlet and exit) temperatures are used to calculate a mean temperature in each segment, T_m. The local convective heat transfer coefficients, *h* ($Wm^{-2}K^{-1}$) are calculated using temperatures T_w and T_m:

$$h = \frac{\varphi}{(T_w - T_m)} \quad (3)$$

The local Nusselt numbers are then calculated using Eq. (4), taking into consideration the slight evolution in the fluid thermal conductivity κ ($Wm^{-1}K^{-1}$) with increased temperature:

$$Nu = \frac{hD}{\kappa} \quad (4)$$

Figure 4 shows the spatial evolution of the local Nusselt number calculated for different Reynolds numbers in both configurations. On the top horizontal axes, the inclined gray segments represent the vortex generator locations, and the black dots show the thermocouple positions. The experimental data uncertainties are determined and the maximum uncertainty associated with the Nusselt number is estimated at 2.5%. The longitudinal increase of the Nusselt number is related to the increase in heat transfer coefficient, *h*, produced by the flow hydrodynamics. Each row of trapezoidal tabs regenerates the vortex pairs continuously, sustaining the radial transport phenomena that carry hot fluid from the wall region to the core flow homogenizing the cross-sectional temperature and increasing the heat exchange between hot and cold fluid zones. The convective heat transfer is also promoted by the increase in the Reynolds number. The turbulent structures thus created in the flow replace the parallel laminar streamlines, enhance fluid mixing and intensify the effect of the embedded vortical structures to produce higher Nusselt numbers. As shown in Fig. 4(a), local Nusselt numbers in the Reversed Arrays configuration have a tendency to increase in the longitudinal direction throughout the entire exchanger length, whereas in the Aligned Arrays, the values increase up to the fifth tab array after which the curve seems to reach a plateau. The experimental data confirm previous hydrodynamic and thermal numerical results in the Aligned Arrays configuration where the local Nusselt numbers and the turbulent kinetic energy, produced by the detachment of the shear layer from the tab's edge, were found to increase up to the fourth tab array.[13,14] The high-energy structures in the Reversed Arrays configuration and the abrupt impact with the upstream sharp tab edge delay the stabilization of *Nu* in this geometry by maintaining high levels of molecular scale agitation that contributes to the overall thermal enhancement.

In both configurations, it can be seen that local convective heat transfer in the zone between the wall and the tab root is weaker than further downstream. Low-velocity recirculation zones prevail in this region and most of the hydrodynamic effects of the vortex generators fully develop downstream from the tab's tip where, in the Aligned Arrays, the hairpin vortices are produced due to the Kelvin-Helmholtz instability, and in the Reverse Arrays, high levels of turbulent kinetic energy dissipation rates are recorded, in addition to the necklace vortices.

Also, the tab's temperature is close to that of the wall and thus it acts as a thermal fin and injects additional heat into the flow. The average standard deviation of the local Nusselt numbers from the mean values, that are represented by the smoothed curves of Fig.4, is around 12% for the Reversed Arrays and 7% for the Aligned Arrays owing to the fact that in the first configuration, most of the flow activity is localized around the tabs and the downstream CVP are attenuated faster than in the case of Aligned Arrays where transfer is more uniform.

Figure 5 gives further details about the local variations of the Nusselt number within the cross-section

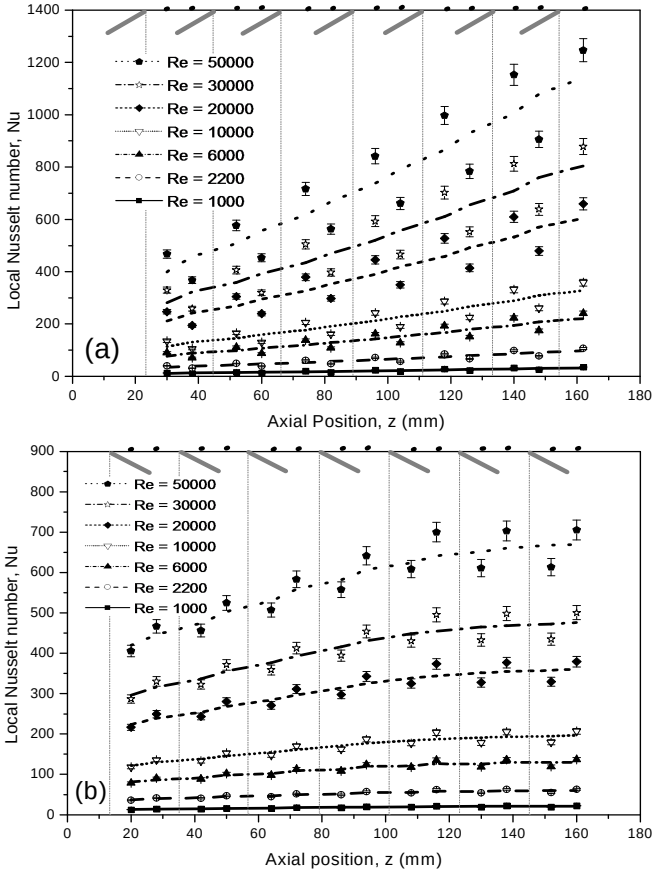

Fig. 4. Local Nusselt number for different Re: (a) Reversed Arrays and (b) Aligned Arrays

and allows for a more accurate estimation of the global quantities. It can be seen that, in the Reversed Arrays, the local Nusselt number values measured at an angular position 45°away from the tab location are 13% higher than those recorded in the zone aligned with the tabs (0°). For the Aligned arrays, the average difference is 10% for the entire range of Reynolds numbers run. This deviation can be interpreted by the propagation of the primary CVP away from the tab edges into the core flow, together with the reduced heat exchange in the recirculation zones between the tab root and the wall. The global influence of the different zones and flow structures on the overall heat transfer character of the HEV compared to other devices is discussed in the following section.

3.2. Global Analysis

The thermal performance of a heat exchanger can be defined by the global convective heat transfer coefficient h_g or the global Nusselt number Nu_g, which represents the ratio of convective to conductive heat transfer. Figure 6 shows the variation of global Nusselt number with Reynolds number. The results confirm those of previous numerical studies [2,19] which showed a great increase of the Nusselt number with Reynolds number. For all experiments in the current study, Nusselt number increases with Reynolds number. This increase is attributed, among other parameters, particularly to the enhancement of turbulence intensity.

The Gnielinski equation [15] (Eq. (5)) gives a correlation for Nusselt number in turbulent tube flow Nu_0

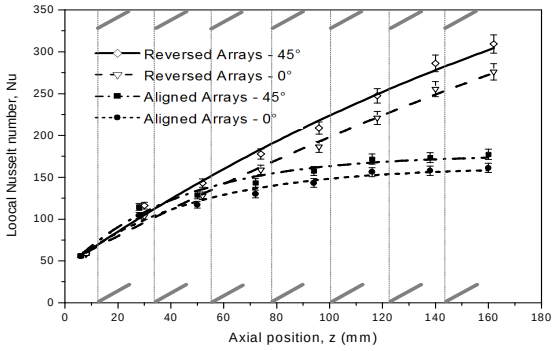

Fig. 5. Local Nusselt number for Re = 8000

for Prandtl numbers *Pr* ranging from 0.5 to 200 and Reynolds numbers from 2300 to 5×10^6:

$$Nu_0 = \frac{(f_0/8)(Re-1000)Pr}{1+12.7(f_0/8)^{1/2}(Pr^{2/3}-1)} \quad (5)$$

where f_0 is the friction factor in a smooth-pipe turbulent flow given by the Petukhov correlation:

$$f_0 = [0.79\ln(Re)-1.64]^{-2} \quad (6)$$

The numerical study of Mohand Kaci et al. [14] predicts a 500% increase in average convective heat transfer in the HEV flow over a turbulent tube flow. For a matching range of Reynolds numbers (7500<Re<15000), the experimental results are in good agreement with the numerical predictions. The present study, however, provides heat transfer information on a much wider range of flow regimes and Reynolds numbers.

The highest relative enhancement is produced in the transitional regime for 1400<Re<4000 where the relative enhancement reaches values up to 1100% in the Reversed Arrays and 880 % in the Aligned Arrays, decreasing gradually, to reach 450% and 310% respectively, as the regime becomes more turbulent and the natural vortical structures enhance heat transfer in the plain tube without the need for artificial turbulence production.

The increase of Nusselt number with Reynolds number in the HEV is strongly accelerated over that in the plain tube by the destruction of the boundary layer at each tab array. It should be noted that the internal convective heat transfer does not reach a saturation plateau, meaning that the thermal boundary layers are not fully developed inside the tube length; this information should be useful in heat exchanger design. The global Nusselt numbers in the Reversed Arrays configuration are around 22% higher than those in the Aligned Arrays due to higher flow vorticity and TKE dissipation rates.

Taking into consideration the variation of the thermophysical properties of water, the plot of $Nu/Pr^{0.4}$ versus *Re* gives the ad hoc correlations for Nusselt number in the Reversed Arrays and the Aligned Arrays configurations given by Eq.s (7) and (8) respectively:

$$Nu_g = 0.0321 Re^{0.861} Pr^{0.4} \quad (7)$$

$$Nu_g = 0.0385 Re^{0.813} Pr^{0.4} \quad (8)$$

These correlations describe the thermal behavior of the HEV flow over the range of Reynolds numbers studied and can be used as a design rule in new HEV heat exchangers applications.

Another criterion for judging the energy efficiency of a heat exchanger is the Colburn factor *j*, given by

$$j = \frac{Nu}{RePr^{1/3}} \quad (9)$$

The Colburn factor quantifies the ratio of the thermal power transferred to the mechanical power consumed. For a given fluid and a specific range of Reynolds number, a higher Colburn factor indicates a higher quality of heat transfer. Figure 7 shows a classification of commercial heat exchangers in terms of this factor revealing the remarkable performance of the HEV heat exchanger, especially the Reversed Arrays configuration, compared to other devices. However, in order to achieve a comprehensive characterization of the net gain, the next section discusses the friction factor and the energy efficiency of the HEV configurations.

3.3. Friction Factor and Thermal Performance

The Fanning friction factor *f* is related to pressure losses by the Darcy-Weisbach equation (Eq. 10). Based on differential pressure measurements between the entrance and exit from the HEV heat exchanger, the friction factor is calculated:

$$f = \frac{\Delta P}{4\left(\frac{L}{D}\right)\left(\rho\frac{U_m^2}{2}\right)} \quad (10)$$

where ρ is the fluid density (kgm^{-3}). The ratio of the HEV flow friction factor to that in a plain tube flow (f_0) is plotted in Fig. 8 against Re. Not surprisingly, the presence of the tab rows generates additional losses by friction due to a greater blockage and flow interruption and thus increased

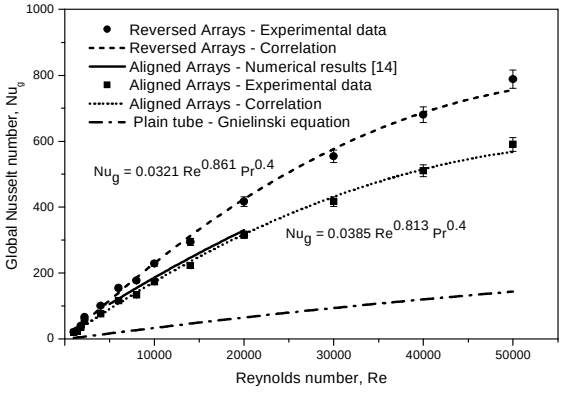

FIG. 6. Global Nusselt number versus Re

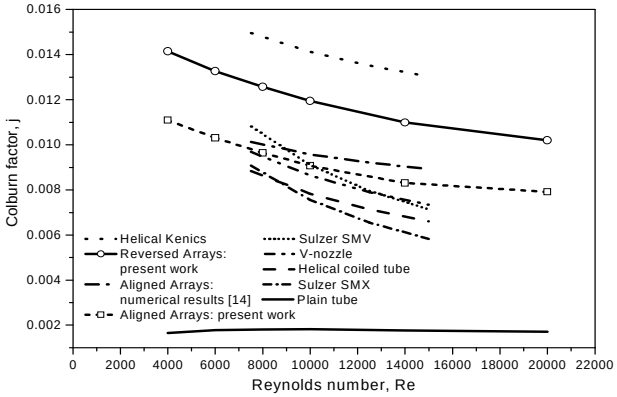

FIG. 7. Colburn factor for commercial heat exchangers [14]

inertial forces in the boundary layer. The relative friction factor values are high in the laminar regime due to the presence of the tabs independently from the flow inertia. In the transition zone, the plain tube friction factors seem to increase at a higher rate and thus f/f0 has a decreasing tendency in this zone. Turbulence, however, produces higher losses in the HEV due to excessive interaction between the flow and the sharp-edged solid tabs; f/f0 starts to increase starting from Re=4000 but tends to stabilize for higher Re. In the laminar regime, both configurations show similar behavior. For higher Re, friction losses in the Reversed Arrays configuration exceed those in the Aligned Arrays. The fluid stream abruptly encounters the reversed tab edges and does not have sufficient time to change its direction and smoothly follow the solid structure, as in the case of Aligned Arrays, ultimately contributing to increased interaction

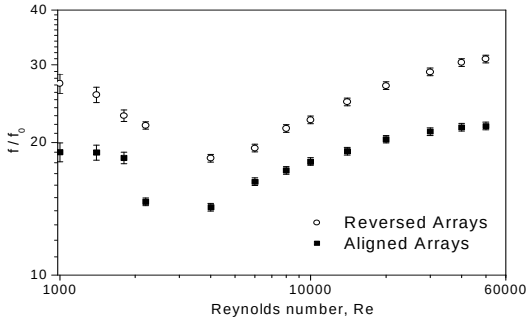

Fig. 8. Variation of friction factor ratio, HEV/plain tube

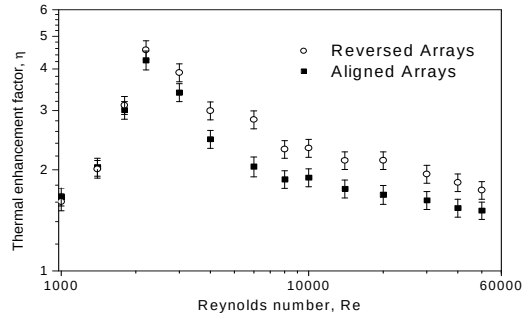

Fig. 9. Thermal enhancement factor versus Re

with the tab surface and higher energy dissipation.

From a process engineering perspective, the feasibility of a heat exchanger can only be assessed through simultaneous consideration of heat transfer gain and pumping costs. The thermal enhancement factor η is defined as the ratio of the surface heat transfer coefficient in the modified geometry h to that of a plain surface h_0 at equal pumping power (*pp*) and is given by:

$$\eta = \left.\frac{h}{h_0}\right|_{pp} = \left.\frac{Nu}{Nu_0}\right|_{pp} = \frac{Nu/Nu_0}{\left(f/f_0\right)^{1/3}} \qquad (11)$$

Figure 9 shows the variation of η with Re showing that, for equivalent pumping costs, the HEV configurations exhibit heat transfer rates that are 50% to 500% higher than those in a plain tube depending on the flow regime. A particular interest of using the HEV configurations is in the transition zone where the maximum overall net gain is produced. For higher Reynolds numbers, increased friction losses render the HEV less profitable. The Reversed Arrays configuration reveals a capacity to enhance heat transfer with moderate energy consumption. Albeit, this configuration presents higher fouling potential and might require additional maintenance costs.

4. Conclusions

Convective heat-transfer enhancement in a tube fitted with trapezoidal tabs inclined in the counter-flow direction is experimentally investigated. A global analysis of the results is presented and the energetic costs of the process intensification are assessed. The values of Nusselt number and friction factor in the tube equipped with vorticity generators are higher than those in a plain tube. The vorticity produced in the turbulent flow in the HEV multifunctional heat exchanger-reactor is the main factor behind the enhanced transfer. The pressure drop is tolerable compared to similar devices. The experimental study validates the numerical results of [13,14] and confirms the capacity of the HEV heat exchanger, especially the Reversed Arrays configuration, to improve convective heat transfer while producing moderate pressure losses.

References

[1] Gretta WJ and Smith CR. The flow structure and statistics of a passive mixing tab. Trans. ASME J. Fluids Eng.1993;115:255-263.

[2] Fiebig M. Vortices, generators and heat transfer. Chem. Eng. Res. Des. 1998;76:108–123.

[3] Yang W, Meng H, Sheng J. Dynamics of hairpin vortices generated by a mixing tab in a channel flow. Exp. Fluids 2001;30:705–722.

[4] Dong D and Meng H. Flow past a trapezoidal tab. J. Fluid Mech. 2004;510:219–242.

[5] Lemenand T, Della Valle D, Zellouf Y, Peerhossaini H. Droplets formation in turbulent mixing of two immiscible fluids. Int. J. Multiphase Flow 2003;29:813–840.

[6] Lemenand T, Dupont P, Della Valle D, Peerhossaini H. Turbulent mixing of two immiscible fluids. J. Fluids Eng.-Transactions of the ASME 2005;127 (6):1132-1139.

[7] Ghanem A, Habchi C, Lemenand T, Della Valle D, Peerhossaini H. Energy efficiency in process industry – High-efficiency vortex (HEV) multifunctional heat exchanger. Renew. Energy 2012. In press, doi: 10.1016/j.renene.2012.09.024.

[8] Lemenand T, Durandal, C, Della Valle D, Peerhossaini H. Turbulent direct-contact heat transfer between two immiscible fluids. Int. J. Thermal Sciences 2010;49:1886-1898.

[9] Mohand Kaci H, Lemenand T, Della Valle D., Peerhossaini H. Effects of embedded streamwise vorticity on turbulent mixing. Chem. Eng. Process 2009;48:1457-1474.

[10] Habchi C, Lemenand T, Della Valle D, Peerhossaini H. Alternating mixing tabs in multifunctional heat exchanger-reactor. Chem. Eng. Process 2010;49:653-661.

[11] Habchi C, Russeil S, Bougeard D, Harion JL, Lemenand T, Della Valle D, Peerhossaini H. Enhancing heat transfer in vortex generator-type multifunctional heat exchangers. Appl. Therm. Eng. 2012;38:14-25.

[12] Chemineer, Kenics. Static Mixing Technology, Bulletin 800 (commercial documentation), Chemineer Inc., Dayton, OH,1998.

[13] Habchi C, Lemenand T, Della Valle D, Peerhossaini H. Turbulent mixing and residence time distribution in novel multifunctional heat exchangers-reactors. Chem. Eng. Process 2010;49:1066-1075.

[14] Mohand Kaci H, Habchi C, Lemenand T, Della Valle D, Peerhossaini H. Flow structure and heat transfer induced by embedded vorticity. Int. J Heat Mass Trans. 2010;53:3575-3584.

[15] Gnielinski V. New equations for heat and mass transfer in turbulent pipe flow. Int. Chem. Eng.1976;16:359–368.